Simulation of the electron-phonon interaction in infinite dimensions

J. K. Freericks

Department of Physics, University of California, Davis, CA 95616

M. Jarrell

Department of Physics, University of Cincinnati, Cincinnati, OH 45221

Abstract. The electron-phonon interaction corresponding to the Holstein model (with Coulomb repulsion) is simulated in infinite dimensions using a novel quantum Monte Carlo algorithm. The thermodynamic phase diagram includes commensurate charge-density-wave phases, incommensurate charge-density-wave phases, and superconductivity. The crossover from a weak-coupling picture (where pairs both form and condense at T_c) to a strong-coupling picture (where preformed pairs condense at T_c) is illustrated with the onset of a double-well structure in the effective phonon potential.

1. Infinite-dimensional formalism

Strong electron-electron correlations are responsible for many important and exotic phenomena in condensed-matter systems including superconductivity, magnetism, heavy fermions, *etc.* Strongly correlated electronic systems are those in which the average electronic correlation energy is equal to or larger than the electronic kinetic energy. Exotic phenomena arise from the competition of simultaneously minimizing the kinetic and potential energy of the electrons. Models of these systems usually do not have analytic solutions. However, recently, Metzner and Vollhardt [1] discovered that these many-body problems simplify in the limit of infinite spatial dimensions. The limit must be taken in such a fashion that the electronic kinetic energy remains finite, so that the effects of the strong electron correlations remain.

Consider the electronic kinetic energy determined by a tight-binding model with hopping between nearest-neighbor sites (with hopping integral t) on a hypercubic lattice in d dimensions. The band structure $\epsilon(\mathbf{k})$ becomes

$$\epsilon(\mathbf{k}) = -2t \sum_{i=1}^{d} \cos \mathbf{k}_i \qquad . \tag{1}$$

In the infinite-dimensional limit ($d \to \infty$) the set of $\{\cos \mathbf{k}_i\}$ can be thought of as "random" numbers distributed between -1 and 1 for a general point

in the d-dimensional Brillioun zone. The sum of d "random" numbers grows as $\sqrt{d}$, so the band structure remains finite if the hopping integral scales as $t = t^*/2\sqrt{d}$ [1]. Furthermore the central limit theorem states that the density of states corresponding to this band structure [$\rho(y)$] becomes a Gaussian distribution

$$\rho(y) = \frac{1}{\sqrt{\pi}t^*} \exp\left(-\frac{y^2}{t^{*2}}\right) \quad , \tag{2}$$

in the infinite-dimensional limit. The number of nearest neighbors ($2d$) diverges, but the hopping between nearest neighbors ($t = t^*/2\sqrt{d}$) vanishes in such a fashion to maintain a finite kinetic energy for the electrons.

The phonon density of states has a very different behavior in the infinite-dimensional limit. The phonon density of states for the Debye model (phonons with a linear dispersion from zero frequency to ω_D) is

$$N(\omega) = \frac{C_d}{\omega_D}\left[\frac{\omega}{\omega_D}\right]^{d-1} \quad , \quad 0 \leq \omega \leq \omega_D \quad , \tag{3}$$

in d dimensions. In the limit as $d \to \infty$, the phonon density of states becomes a delta function at the Debye frequency.

These two observations for the electron and phonon densities of states motivate one to examine the Holstein-Hubbard model [2, 3] (in which the electrons couple to localized phonons) as the simplest electron-phonon model in infinite-dimensions:

$$
\begin{aligned}
H &= -\frac{t^*}{2\sqrt{d}} \sum_{\langle j,k\rangle\sigma} (c_{j\sigma}^\dagger c_{k\sigma} + c_{k\sigma}^\dagger c_{j\sigma}) + \sum_j (gx_j - \mu)(n_{j\uparrow} + n_{j\downarrow} - 1) \\
&+ U_c \sum_j (n_{j\uparrow} - \frac{1}{2})(n_{j\downarrow} - \frac{1}{2}) + \frac{1}{2}M\Omega^2 \sum_j x_j^2 + \frac{1}{2}\sum_j \frac{p_j^2}{M} \quad .
\end{aligned}
\tag{4}
$$

Here $c_{j\sigma}^\dagger$ ($c_{j\sigma}$) creates (destroys) an electron at site j with spin σ, $n_{j\sigma} = c_{j\sigma}^\dagger c_{j\sigma}$ is the electron number operator, and x_j (p_j) is the phonon coordinate (momentum) at site j. The hopping matrix elements connect the nearest neighbors of a hypercubic lattice in d-dimensions and the unit of energy is chosen to be this rescaled matrix element t^*. The phonon has a mass M (chosen to be $M = 1$), a frequency Ω, and a spring constant $\kappa \equiv M\Omega^2$ associated with it. The electron-phonon coupling constant (deformation potential) is denoted by g so that the effective electron-electron attraction becomes the bipolaron binding energy

$$U \equiv -\frac{g^2}{M\Omega^2} = -\frac{g^2}{\kappa} \quad . \tag{5}$$

The Coulomb repulsion is represented by a local Hubbard interaction U_c and the chemical potential is denoted by μ with particle-hole symmetry occurring for $\mu = 0$.

The observation of Metzner and Vollhardt [1] is that the many-body problem also simplifies in the infinite-dimensional limit—both the self energy and the irreducible vertex functions become independent of momentum, and are functionals of the interacting Green's function [1, 4, 5]. The Green's function, self energy, and irreducible vertices still retain their complicated time (frequency) dependence.

The many-body problem is solved by mapping it onto an auxiliary impurity problem [6, 7] in a time-dependent field that mimics the hopping of an electron onto a site at time τ and off the site at a time τ'. The action for the impurity problem is found by integrating out all of the degrees of freedom of the other lattice sites in a path-integral formalism [8]. The lattice is viewed as a reservoir of electrons that can hop onto and off of the local site. Once an electron hops off of the local site, it never returns, because the number of paths that loop through the local site are a factor of $1/d$ smaller than the number of paths that do not loop through the local site. Therefore, the effective action for the impurity problem becomes

$$
\begin{aligned}
S &= \sum_\sigma \int_0^\beta d\tau \int_0^\beta d\tau' c_\sigma^\dagger(\tau) G_0^{-1}(\tau - \tau') c_\sigma(\tau') \\
&+ \sum_\sigma \int_0^\beta d\tau [gx(\tau) - \mu][n_\sigma(\tau) - \frac{1}{2}] \\
&+ U_c \int_0^\beta d\tau [n_\uparrow(\tau) - \frac{1}{2}][n_\downarrow(\tau) - \frac{1}{2}] + \frac{M}{2} \int_0^\beta d\tau [\Omega^2 x^2(\tau) + \dot{x}^2(\tau)] \quad (6)
\end{aligned}
$$

where G_0^{-1} is the "bare" Green's function that contains *all of the dynamical information of the other sites of the lattice.* The interacting Green's function, defined to be

$$
G(i\omega_n) \equiv \int_0^\beta d\tau e^{i\omega_n \tau} G(\tau) \quad , \quad G(\tau) = -\frac{\mathrm{Tr}\langle e^{-\beta H} T_\tau c(\tau) c^\dagger(0)\rangle}{\mathrm{Tr}\langle e^{-\beta H}\rangle} \quad , \tag{7}
$$

then satisfies Dyson's equation

$$
G_n^{-1} \equiv G^{-1}(i\omega_n) = G_0^{-1}(i\omega_n) - \Sigma(i\omega_n). \tag{8}
$$

A self-consistency relation is required in order to determine the bare Green's function G_0. This is achieved by mapping the impurity problem onto the infinite-dimensional lattice thereby equating the full Green's function for the impurity problem with the local Green's function for the lattice

$$
\begin{aligned}
G_{jj}(i\omega_n) &= \sum_{\mathbf{k}} G(\mathbf{k}, i\omega_n) = \sum_{\mathbf{k}} [i\omega_n + \mu - \epsilon(\mathbf{k}) - \Sigma(i\omega_n)]^{-1} \\
&= F_\infty[i\omega_n + \mu - \Sigma(i\omega_n)]. \tag{9}
\end{aligned}
$$

Here $F_\infty(z)$ is the scaled complimentary error function of a complex argument.

$$
\begin{aligned}
F_\infty(z) &\equiv \frac{1}{\sqrt{\pi}} \int_{-\infty}^{\infty} dy \frac{\exp(-y^2)}{z-y} \\
&= -i\,\text{sgn}[\text{Im}(z)]\sqrt{\pi}e^{-z^2}\text{erfc}\{-i\,\text{sgn}[\text{Im}(z)]z\}.
\end{aligned} \tag{10}
$$

The dynamics of the (local) impurity problem is identical to the dynamics of the Anderson impurity model [4, 6, 7, 8, 9]. This many-body problem can be solved exactly with the quantum Monte Carlo (QMC) algorithm of Hirsch and Fye [10] (see the next section). The impurity is self-consistently embedded in the host, since it must satisfy the self-consistency relation in Eq. (9). Note that this mapping of the infinite-dimensional lattice problem onto a single-site impurity problem is in the *thermodynamic limit*. There are no finite-size effects in infinite-dimensions.

Static two-particle properties are also easily calculated since the irreducible vertex function is local [11]. The static susceptibility for CDW order is given by

$$
\begin{aligned}
\chi^{CDW}(\mathbf{q}) &\equiv \frac{1}{2N} \sum_{jk\sigma\sigma'} e^{i\mathbf{q}\cdot(\mathbf{R}_j-\mathbf{R}_k)} T \int_0^\beta d\tau \int_0^\beta d\tau' \\
&\qquad\qquad [\langle n_{j\sigma}(\tau)n_{k\sigma'}(\tau')\rangle - \langle n_{j\sigma}(\tau)\rangle\langle n_{k\sigma'}(\tau')\rangle] \\
&\equiv T \sum_{mn} \tilde{\chi}^{CDW}(\mathbf{q},i\omega_m,i\omega_n) = T \sum_{mn} \tilde{\chi}_{mn}^{CDW}(\mathbf{q}) \quad,
\end{aligned} \tag{11}
$$

at each ordering wavevector $\mathbf{q}$. Dyson's equation for the two-particle Green's function becomes [9, 11]

$$
\tilde{\chi}_{mn}^{CDW}(\mathbf{q}) = \tilde{\chi}_m^0(\mathbf{q})\delta_{mn} - T \sum_p \tilde{\chi}_m^0(\mathbf{q})\Gamma_{mp}^{CDW}\tilde{\chi}_{pn}^{CDW}(\mathbf{q}) \quad, \tag{12}
$$

with Γ_{mn}^{CDW} the (local) irreducible vertex function in the CDW channel.

The bare CDW susceptibility $\tilde{\chi}_n^0(\mathbf{q})$ in Eq. (12) is defined in terms of the dressed single-particle Green's function

$$
\begin{aligned}
\tilde{\chi}_n^0(\mathbf{q}) &\equiv -\frac{1}{N} \sum_{\mathbf{k}} G_n(\mathbf{k})G_n(\mathbf{k}+\mathbf{q}) = -\frac{1}{\sqrt{\pi}} \frac{1}{\sqrt{1-X^2}} \\
&\qquad \times \int_{-\infty}^{\infty} dy \frac{e^{-y^2}}{i\omega_n + \mu - \Sigma_n - y} F_\infty\left[\frac{i\omega_n + \mu - \Sigma_n - Xy}{\sqrt{1-X^2}}\right]
\end{aligned} \tag{13}
$$

and all of the wavevector dependence is included in the scalar [6, 12] $X(\mathbf{q}) \equiv \sum_{j=1}^d \cos \mathbf{q}_j/d$. The mapping $\mathbf{q} \mapsto X(\mathbf{q})$ is a many-to-one mapping that determines an equivalence class of wavevectors in the Brillouin zone. "General" wavevectors are all mapped to $X=0$ since $\cos \mathbf{q}_j$ can be thought of as a random number between -1 and 1 for "general" points in the Brillouin zone. Furthermore, all possible values of X $(-1 \le X \le 1)$ can be labeled by a wavevector

that lies on the diagonal of the first Brillouin zone extending from the zone center ($X = 1$) to the zone corner ($X = -1$). The irreducible vertex function Γ_{mn}^{CDW} is determined by inverting the Dyson equation in Eq. (12) for the *local* susceptibility (which is determined by the Monte Carlo techniques of the following section). Once the irreducible vertex function is found, then Eq. (12) is employed to calculate the momentum-dependent susceptibility.

A similar procedure is used to explore the superconductivity of the model. Here, as in the Hubbard model, it is only necessary to look for superconductivity with the same symmetry as the lattice (s-wave) since other superconductivity with other symmetries do not have pairing interactions [13]. For the singlet *s*-wave SC channel, the corresponding definitions are as follows: The static susceptibility in the superconducting channel is defined to be

$$
\begin{aligned}
\chi^{SC}(\mathbf{q}) &\equiv \frac{1}{N} \sum_{jk} e^{i\mathbf{q}\cdot(\mathbf{R}_j - \mathbf{R}_k)} T \int_0^\beta d\tau \int_0^\beta d\tau' \langle c_{j\uparrow}(\tau) c_{j\downarrow}(\tau) c_{k\downarrow}^\dagger(\tau') c_{k\uparrow}^\dagger(\tau') \rangle \\
&\equiv T \sum_{mn} \tilde{\chi}^{SC}(\mathbf{q}, i\omega_m, i\omega_n) = T \sum_{mn} \tilde{\chi}_{mn}^{SC}(\mathbf{q}) \quad,
\end{aligned}
\tag{14}
$$

for superconducting pairs that carry momentum $\mathbf{q}$; Dyson's equation becomes

$$
\tilde{\chi}_{mn}^{SC}(\mathbf{q}) = \tilde{\chi}_m^{0\,\prime}(\mathbf{q})\delta_{mn} - T \sum_p \tilde{\chi}_m^{0\,\prime}(\mathbf{q}) \Gamma_{mp}^{SC} \tilde{\chi}_{pn}^{SC}(\mathbf{q}) \quad,
\tag{15}
$$

with Γ_{mn}^{SC} the corresponding irreducible vertex function for the SC channel; the bare pair-field susceptibility becomes

$$
\begin{aligned}
\tilde{\chi}_n^{0\,\prime}(\mathbf{q}) &\equiv \frac{1}{N} \sum_{\mathbf{k}} G_n(\mathbf{k}) G_{-n-1}(-\mathbf{k} + \mathbf{q}) = \frac{1}{\sqrt{\pi}} \frac{1}{\sqrt{1 - X^2}} \\
&\quad \times \int_{-\infty}^\infty dy \frac{e^{-y^2}}{i\omega_n + \mu - \Sigma_n - y} F_\infty \left[\frac{-i\omega_n + \mu - \Sigma_n^* - Xy}{\sqrt{1 - X^2}} \right]
\end{aligned}
\tag{16}
$$

with the special value $\tilde{\chi}_n^{0\,\prime}(X = 1) = -\mathrm{Im}G_n/\mathrm{Im}(i\omega_n - \Sigma_n)$ for the SC pair that carries no net momentum; and finally the irreducible vertex function is also determined by inverting the Dyson equation in Eq. (15) for the *local* susceptibility.

2. Monte Carlo Algorithm

The dynamics of the impurity problem are identical to that of an impurity embedded in a host metal described by the "bare" Green's function G_0 [4, 8, 9]. Thus, given G_0, the impurity problem may be solved by using the quantum Monte Carlo (QMC) algorithm of Hirsch and Fye [10] (an alternative derivation of this algorithm is presented in the appendix). In the QMC the problem is cast into a discrete path formalism in imaginary time, τ_l, where $\tau_l = l\Delta\tau$,

$\Delta\tau = \beta/L$, and L is the number of times slices. The values of L used ranged from 40 to 160, with the largest values of L reserved for the largest values of β because the time required by the algorithm increases like L^3. Since the bare Green's function G_0^{-1} in Eq. (8) is not *a priori* known, the QMC algorithm must be iterated to determine a self-consistent solution for the Green's function of the infinite-dimensional lattice. The procedure [9] is to begin with a bare Green's function G_0^{-1}, use the QMC algorithm to determine the self energy Σ, calculate the lattice Green's function from Eq. (9), and determine a new bare Green's function from Eq. (8). This process is iterated until convergence is reached (typically $7 - 9$ iterations). At each step, the precision (the total number of field-configurations generated) is increased. In addition, results from high temperature runs are used to initialize lower temperature runs. These last two steps, are commonly used to to anneal out the state with the lowest free energy.

The details of the (Hirsch-Fye [10]) impurity algorithm, as modified for the Holstein-Hubbard model, are reproduced in the appendix. For the remainder of this section, we will discuss the modifications necessary to apply this algorithm to the infinite-dimensional limit. The main difficulty is that the Hirsch-Fye algorithm requires an imaginary-time path integral technique which only produces data for $G(\tau)$ at a *discrete* set of points in Euclidean time $0 < \tau < \beta$; whereas, the self-consistency step requires either the Matsubara frequency Green's function or the corresponding self energy. This involves a numerical approximation of the integral in Eq. (7). Fourier transforming discretely sampled data presents some well known difficulties [14]. The principle difficulty is that Nyquist's theorem tells us that above some frequency $\omega_n = 1/2\Delta\tau$, unpredictable results are produced by conventional quadrature techniques. Typically this problem is overcome by fitting the discrete data $G(\tau)$ with a smooth cubic spline, and then performing the integral on the splined data [14]. Since the integral on the splined data may be sampled on a much finer grid than the original data, this process is referred to as over sampling.

However, a problem still remains at high frequencies, since the resulting $G(i\omega_n)$ goes quickly to zero for frequencies above the Nyquist cutoff $1/2\Delta\tau$. This presents a difficulty since causality requires that

$$\lim_{\omega_n \to \infty} G(i\omega_n) \sim \frac{1}{i\omega_n} \, . \tag{17}$$

In order to maintain causality [15] of the Matsubara frequency Green's functions, we condition the Fourier transform with a perturbation theory result. That is, we write

$$G(i\omega_n) = G_{pt}(i\omega_n) + \int_0^\beta d\tau e^{i\omega_n \tau} \left(G(\tau) - G_{pt}(\tau) \right) \, . \tag{18}$$

where G_{pt} is a Green's function obtained from perturbation theory, and the integral here is performed by the oversampling method described above.

There are two obvious advantages to this approach. First, the integral goes to zero for frequencies greater than the Nyquist frequency $1/2\Delta\tau$, so that the resulting Green's function has the same asymptotic behavior as the perturbation theory result, and is thus causal. Second, often, the perturbation theory result is asymptotically exact (*i. e.* results from a high temperature expansion *etc.*), and this then presents a way of appending exact QMC results at low frequency with asymptotically exact perturbation theory results at high frequency. The flow chart for the resulting algorithm is shown in Fig. 1.
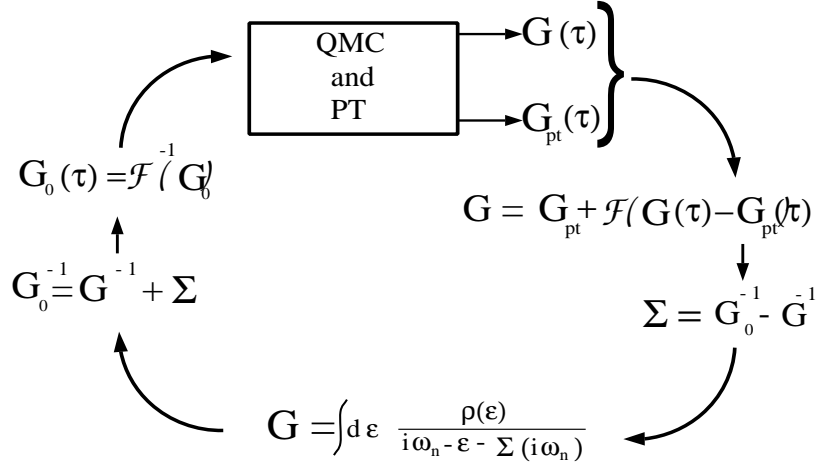

Figure 1. *Flowchart for the $d = \infty$ algorithm. The symbol $\mathcal{F}$ denote that a Fourier transform is to be performed by oversampling, and $\mathcal{F}^{-1}$ denotes its inverse.*

Once convergence of the algorithm in Fig. 1 is reached, the physical properties of the system are calculated with the QMC. A variety of two-particle properties may be calculated in the QMC approach since the irreducible vertex function is also local. For most quantities, this is straight-forward; however, the two-particle Green's functions χ_{mn}^{loc} are difficult to measure efficiently. For example, consider the local opposite-spin particle-particle propagator

$$\chi_{nm}^{loc} = \int_0^\beta d\tau_1 \cdots d\tau_4 e^{[i\omega_m(\tau_2-\tau_1)-i\omega_n(\tau_3-\tau_4)]}$$
$$\times \langle T_\tau c_\uparrow(\tau_4)c_\downarrow(\tau_3)c_\downarrow^\dagger(\tau_2)c_\uparrow^\dagger(\tau_1)\rangle. \qquad (19)$$

For a particular configuration of the Hubbard-Stratonovich fields, the Fermions are noninteracting, thus the expectation value indicated by the angle brackets above may be evaluated in two steps. First, using Wick's theorem, its value

is tabulated for each field configuration $\{s_l, x_l\}$. Second, using Monte Carlo techniques these configurations are averaged over. After the first step, the equation becomes

$$\chi^{loc}_{nm} = \left\langle \int_0^\beta d\tau_1 \cdots d\tau_4 e^{[i\omega_m(\tau_2-\tau_1)-i\omega_n(\tau_3-\tau_4)]} g_\uparrow(\tau_4,\tau_1)g_\downarrow(\tau_3,\tau_2) \right\rangle_{m.c.} \quad (20)$$

where the $m.c.$ subscript means that the Monte Carlo average is still to be performed.

To measure this on the computer, the integrals must be approximated by sums. Since the Green's functions change discontinuously when the two time arguments intersect, the best integral approximation that can be used here is the trapezoidal approximation. Using this, we will run into Green's functions with both time arguments the same $g(j,j)$. This is stored as $g(j^+,j)$ (i.e. it is assumed that the first time argument is slightly greater than the second), but in the sums we clearly want the equal time Green's function to be the average $\{g(j^+,j) + g(j,j^+)\}/2 = g(j^+,j) - 1/2$. If we call $\mathbf{g}$, with $1/2$ subtracted from its diagonal elements, $\overline{\mathbf{g}}$, then

$$\chi^{loc}_{nm} = \left\langle \left(\sum_{j,k} \Delta\tau\, e^{+i\pi j(2n+1)/L} \overline{g}_\uparrow(j,k)\, \Delta\tau\, e^{-i\pi k(2m+1)/L} \right) \right. \quad (21)$$
$$\left. \left(\sum_{p,q} \Delta\tau\, e^{-i\pi p(2n+1)/L} \overline{g}_\downarrow(p,q)\, \Delta\tau\, e^{+i\pi q(2m+1)/L} \right) \right\rangle_{m.c.}$$

This measurement may be performed efficiently if each term in parenthesis is tabulated first and stored as a matrix, and then the direct product of the two matrices taken as the estimate of χ^{loc}. When done this way, the time required for this measurement scales like $\sim L^3$ rather than $\sim L^4$ as would result from a straight-forward evaluation of the sums implicit in Eq. (20).

Finally, the irreducible vertex function is determined by inverting the relevant local Dyson equation. The momentum-dependent susceptibility may then be calculated from Eq. (12) or (15).

3. Results

For the results presented here, we chose an intermediate phonon frequency $\Omega = 0.5t^*$ (which is approximately one-eight of the effective electronic bandwidth) for which there is a competition between CDW and SC order. As shown in Fig. 3, CDW order is favored near half filling (due to Fermi surface nesting) and SC order is favored away from half filling. As shown in Fig. 2b, there is a maximum CDW transition temperature, because it decreases as the coupling strength increases in the strong-coupling regime.
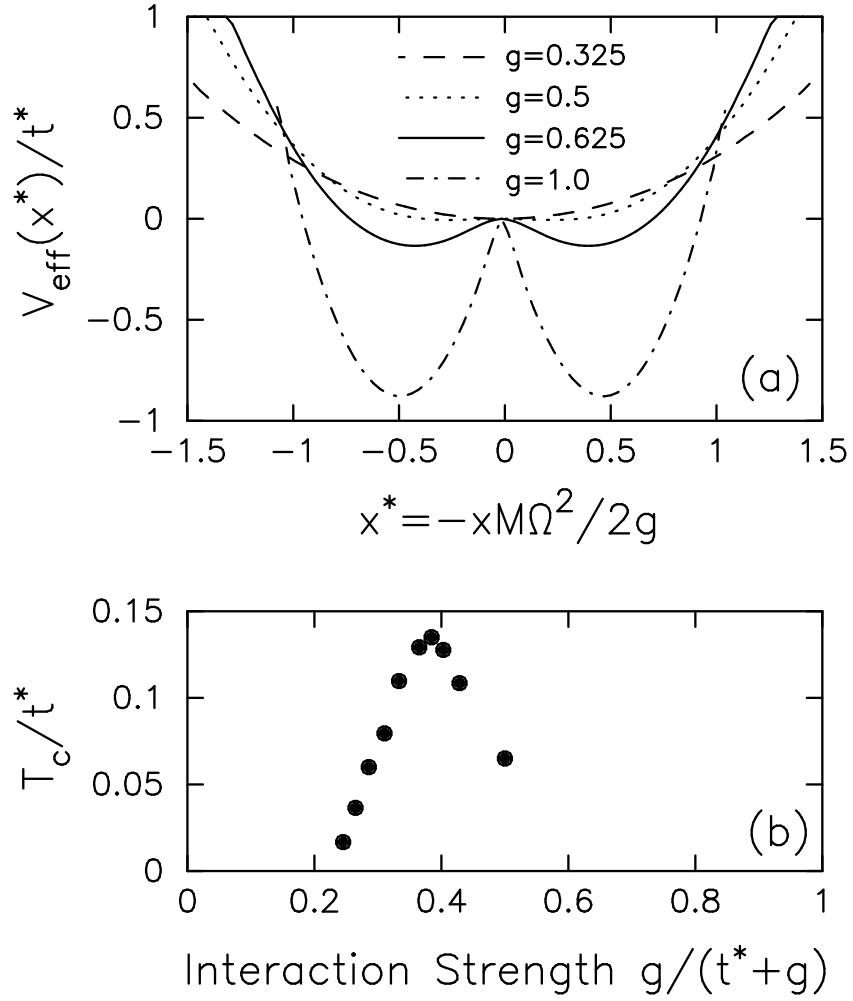
Figure 2: *(a) Effective potential for the phonon (after integrating out the effects of the electrons) as a function of electron-phonon coupling and (b) the CDW transition temperature at half filling as a function of the coupling. The parameters chosen here are $\Omega = 0.5t^*$ and $U_c = 0$. Note that the maximum in the T_c curve occurs when the barrier height of the double-well potential is equal in magnitude to T_c.*

In order to shed some light on the transition from weak to strong coupling the QMC simulations were sampled to determine a time-averaged effective phonon potential. The probability $P(x)$ that the phonon coordinate $x(\tau_\ell)$ lies in the interval from x to $x + \delta x$ was calculated for each time slice τ_ℓ and averaged over all time slices. An effective phonon potential $V_{eff.}(x)$ was then extracted from the probability distribution $P(x) \propto \exp[-\beta V_{eff.}(x)]$ [17]. This effective potential is plotted in Fig. 2 (a) for four different values of the electron-phonon coupling strength at a temperature $T = 1/7$. In the case of weak coupling ($g = 0.325$), the potential appears harmonic. The potential flattens when $U \approx t^*$ ($g = 0.5$) and as g increases further, a double-well structure develops [18]. The barrier height grows linearly with g as does the separation of the minima. The peak of the $T_c(g)$ curve for the CDW transition [see Fig. 2(b)] is reached at the point where the barrier height is on the order of T_c ($g = 0.625$). Beyond this point ($g = 1.0$) the system enters the strong-coupling regime and T_c decreases.

In the region where the double-well potential has developed, the phonon coordinate tunnels between the wells and the tunneling rate decreases as the temperature is lowered below the barrier height. At this point the system may be considered to be a random mixture of empty sites and bipolarons that fluctuates in time. Tunneling through the barrier produces correlations between the empty-sites and the bipolarons resulting in a condensed CDW phase. However as the barrier height increases, the transition temperature drops because the tunneling is suppressed. The transition temperature reaches its maximum at the point where the barrier height is equal in magnitude to T_c.

As the system is doped away from half-filling there is a competition between CDW order and superconductivity . We find that the CDW-ordered state remains "locked" at the "antiferromagnetic" point ($X = -1$) for a wide range of dopings away from half-filling. Figure 3 displays the results for the transition temperature of the Holstein-Hubbard model as a function of electron concentration for two different values of U_c at $g = 0.5t^*$. In the case where $U_c = 0$ the system must be doped out to a concentration of $\rho_e = 0.52$ before it becomes superconducting. There was no evidence for any incommensurate order when $U_c = 0$. We expect that a Coulomb repulsion will favor the SC phase over the CDW phase because the Coulomb repulsion directly reduces the CDW interaction, but is not as effective at reducing the SC interaction because of the retardation between the pairing electrons which allows the electrons to attract each other without being at the same site at the same time (the so-called pseudopotential effect). This result is clearly seen in Figure 3, where the phase space for the SC order increases when $U_c = 0.5$. Note that a finite Coulomb repulsion also favors the appearance of incommensurate phases, which now can be detected with the QMC techniques.
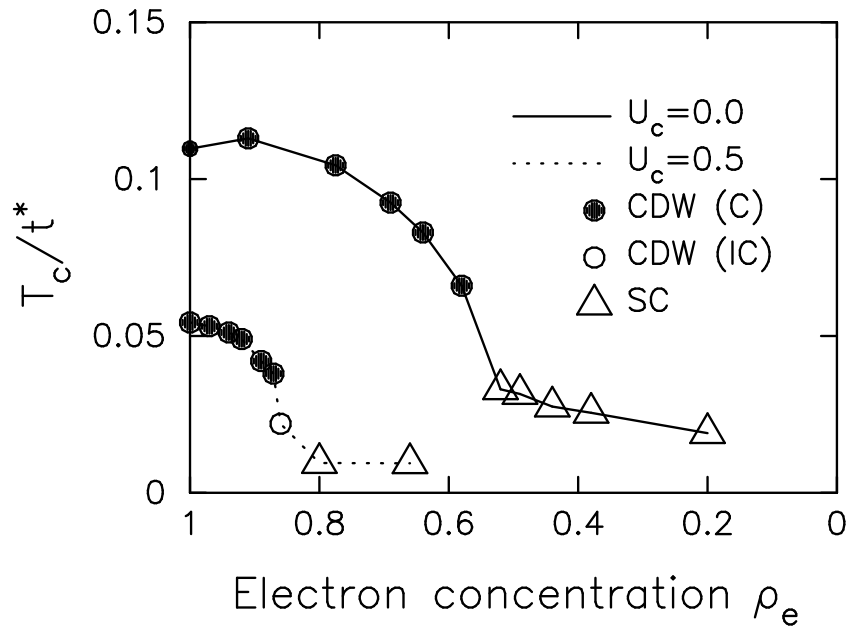
Figure 3: *Transition temperature for the Holstein-Hubbard model at $\Omega = 0.5t^*$ and $g = 0.5t^*$. As the Coulomb repulsion is increased, the SC phase becomes more stable, as do incommensurate CDW phases.*

Appendix. Derivation of Quantum MC algorithm of Hirsch and Fye

The purpose of this section is to derive the Hirsch-Fye algorithm [10] using Grassmann algebra. We begin by splitting the single impurity Anderson model Hamiltonian, into bare and interacting parts, $H = H_0 + H_1 + H_2$, where

$$H_0 = \sum_{k\sigma} \epsilon(\mathbf{k}) c_{k\sigma}^{\dagger} c_{k\sigma} + V \sum_{k\sigma} (f_{\sigma}^{\dagger} c_{k\sigma} + c_{k\sigma}^{\dagger} f_{\sigma})$$

$$+ \quad (gx - \mu)(n_{f\uparrow} + n_{f\downarrow} - 1) + \frac{1}{2} M\Omega^2 x^2 \quad , \tag{22}$$

$$H_1 = U(n_{f\uparrow} - 1/2)(n_{f\downarrow} - 1/2) , \tag{23}$$

and

$$H_2 = \frac{p^2}{2M} . \tag{24}$$

To obtain the Trotter-Suzuki decomposition for the partition function [19] we divide the interval $[0, \beta]$ into L sufficiently small subintervals such that the commutators $\Delta\tau^2 [H_0, H_I]$ *etc.* may be neglected. This leads to

$$Z = Tre^{-\beta H} = Tr \prod_{l=1}^{L} e^{-\Delta\tau H} \approx Tr \prod_{l=1}^{L} e^{-\Delta\tau H_0} e^{-\Delta\tau H_1} e^{-\Delta\tau H_2} . \tag{25}$$

The interacting part of the Hamiltonian, H_1, may be further decoupled by mapping it to an auxiliary Ising field via a discrete Hirsch-Hubbard-Stratonovich [20] transformation,

$$e^{-\Delta\tau H_I} = e^{-\Delta\tau U(n_{f\uparrow} - 1/2)(n_{f\downarrow} - 1/2)} = \frac{1}{2} e^{-\Delta\tau U/4} \sum_{s=\pm 1} e^{\alpha s(n_{f\uparrow} - n_{f\downarrow})} \tag{26}$$

where $\cosh(\alpha) = e^{\Delta\tau U/2}$. Finally, one may cast Eq. (25) into functional-integral form by using coherent states [Grassmann variables for Fermions, and complex numbers for the Bosons, $a = \sqrt{m\Omega/2}(x + ip/m\Omega)$ and a^*]. If we integrate out the host Fermionic degrees of freedom $\{c_{k\sigma}\}$ as well as the momentum of the phonon, then we end up with

$$S_{eff} = (\Delta\tau V)^2 \sum_{l,l',\sigma} f^*_{\sigma,l} G_0(l, l') f_{\sigma,l'} + S_{int} + S_B , \tag{27}$$

where

$$S_B = \frac{\Delta\tau}{2} \sum_l \left[\left(\frac{x_l - x_{l+1}}{\Delta\tau} \right)^2 \right] + \Omega^2 x_l^2 , \tag{28}$$

$$S_{int} = \sum_{l,\sigma,x_l} -f^*_{\sigma,l}(f_{\sigma,l} - f_{\sigma,l-1})$$
$$+ \quad \Delta\tau f^*_{\sigma,l}(gx_l - \mu + \frac{U}{2} + \frac{\alpha}{\Delta\tau} s_l \sigma) f_{\sigma,l-1} \quad , \tag{29}$$

and

$$G_0^{-1}(l, l') = \frac{1}{N} \sum_k \delta_{l,l'} - \delta_{l-1,l'}[1 - \Delta\tau\epsilon(\mathbf{k})] . \tag{30}$$

At this point the correspondence of the impurity and the infinite-dimensional Hubbard model is clear. In both, G_0 contains the information about the host into which the impurity is embedded. The difference is that G_0 must be determined self-consistently for the lattice model.

We will now proceed to derive the Monte Carlo algorithm [10] sufficient for either the impurity or the infinite-dimensional lattice problem. By integrating over $f_{\sigma,l}$ we can write down the partition function (neglecting a numerical prefactor), as

$$Z = \sum_{\{s_l,x_l\}} det(G^{-1}_{\uparrow\{s_l,x_l\}}) det(G^{-1}_{\downarrow\{s_l,x_l\}}) e^{-S_B} \tag{31}$$

where

$$G^{-1}_{\sigma,\{s_l,x_l\}}(l,l') = \delta_{l,l'} - \delta_{l-1,l'}[1 - \Delta\tau\,(gx_l - \mu) + \alpha s_l\sigma] - \Delta\tau^2 V^2 G_0(l,l') \tag{32}$$

and we sum over all configurations of Hubbard-Stratonovich and phonon fields $\{s_l,x_l\}$. If we reexponentiate the above formula by defining $\mathcal{V}_{\sigma,\{s_l,x_l\}}(l) \equiv \Delta\tau(gx_l - \mu + \alpha s_l\sigma/\Delta\tau)$, we can write it in a simple notation as

$$G^{-1}_\sigma = 1 + Te^{\mathcal{V}_\sigma} + \Delta\tau^2 V^2 G_0 \;, \tag{33}$$

where T is $\delta_{l-1,l'}$ and $\mathcal{V}_\sigma \equiv \mathcal{V}_{\sigma,\{s_l,x_l\}}(l)$ for one special configuration. For another field configuration the only difference comes from $\mathcal{V}_\sigma$ such that $G'^{-1}_\sigma - G^{-1}_\sigma = T(e^{\mathcal{V}'_\sigma} - e^{\mathcal{V}_\sigma}) + O(\Delta\tau^{3/2})$ (note that α is of the order of $\Delta\tau^{1/2}$). On the other hand $T = (G^{-1}_\sigma - 1 - \Delta\tau^2 V^2 G_0)e^{-\mathcal{V}_\sigma}$ which results in

$$G'^{-1}_\sigma - G^{-1}_\sigma = (G^{-1}_\sigma - 1)e^{-\mathcal{V}_\sigma}(e^{\mathcal{V}'_\sigma} - e^{\mathcal{V}_\sigma}) + O(\Delta\tau^{3/2})\,. \tag{34}$$

Multiplying from the left by G and from the right by G' and, ignoring terms $O(\Delta\tau^{3/2})$, we find

$$G'_\sigma = G_\sigma + (G_\sigma - 1)(e^{\mathcal{V}'_\sigma - \mathcal{V}_\sigma} - 1)G'_\sigma \;, \tag{35}$$

or

$$G_\sigma G'^{-1}_\sigma = 1 + (1 - G_\sigma)(e^{\mathcal{V}'_\sigma - \mathcal{V}_\sigma} - 1) \quad. \tag{36}$$

The probability of having a configuration $\{s_l,x_l\}$ is $P_{sx} \propto det(G^{-1}_{\uparrow\{s_l,x_l\}}) \times det(G^{-1}_{\downarrow\{s_l,x_l\}}) e^{-S_B}$; on the other hand the detailed balance requires

$$P_{sx'} P_{sx'\to sx} = P_{sx} P_{sx\to sx'} \quad, \tag{37}$$

for all sx'. We may satisfy this requirement by defining the probability of going from $\{s_l,x_l\}$ to $\{s'_l,x'_l\}$ as $R/(1+R)$, where

$$R \equiv \frac{det(G'_\uparrow) det(G'_\downarrow) e^{-S'_B}}{det(G_\uparrow) det(G_\downarrow) e^{-S_B}} \tag{38}$$

is the relative weight of two configurations. If the difference between two configuration is due to a flip of a single Hirsch-Hubbard-Stratonovich field at the mth imaginary time slice then [10]

$$R = \prod_\sigma [1 + (1 - G_{\sigma m,m})(e^{-2\alpha\sigma s_m} - 1)] \,, \tag{39}$$

or, if the difference is due to a change in the phonon displacement $x_l \rightarrow x'_l$, then

$$R = e^{S'_B - S_B} \prod_\sigma [1 + (1 - G_{\sigma m,m})(e^{\Delta\tau g(x_l - x'_l)} - 1)] \,. \tag{40}$$

Finally we can write down the evolution of the Green's function in the QMC time, when for example we flip a single Hirsch-Hubbard-Stratonovich field at the mth imaginary time slice [10]

$$\begin{aligned} G'_{\sigma i,j} &= G_{\sigma i,j} + (G_{\sigma i,m} - \delta_{i,m})(e^{-2\alpha\sigma s_m} - 1) \\ &\times \{1 + (1 - G_{\sigma m,m})(e^{-2\alpha\sigma s_m} - 1)\}^{-1} G_{\sigma m,j} \,. \end{aligned} \tag{41}$$

Similarly, when we change a single boson x_m at the mth time slice,

$$\begin{aligned} G'_{\sigma i,j} &= G_{\sigma i,j} + (G_{\sigma i,m} - \delta_{i,m})(e^{\Delta\tau g(x_l - x'_l)} - 1) \\ &\times \{1 + (1 - G_{\sigma m,m})(e^{\Delta\tau g(x_l - x'_l)} - 1)\}^{-1} G_{\sigma m,j} \,. \end{aligned} \tag{42}$$

The QMC process precedes by sequentially proposing changes in each field, accepting these changes with probability $P_{sx->sx'}$, and updating the Green's function with Eq. (41) or Eq. (42) when the change is accepted. In addition to using local moves in which a single spin or a single phonon field is changed, we also employ global moves, in which either all of the spins are flipped, or all of the phonon coordinates are shifted,

References

[1] W. Metzner and D. Vollhardt, Phys. Rev. Lett. **62**, 324 (1989).

[2] T. Holstein, Ann. Phys. **8**, 325 (1959).

[3] J. Hubbard, Proc. Royal Soc. London (Ser. A) **276**, 238 (1963).

[4] H. Schweitzer and G. Czycholl, Z. Phys. B **77**, 327 (1990).

[5] W. Metzner, Phys. Rev. B **43**, 8549 (1991).

[6] U. Brandt and C. Mielsch, Z. Phys. B **75**, 365 (1989).

[7] F. J. Ohkawa, Phys. Rev. B **44**, 6812 (1991); Prog. Theor. Phys. Suppl. **106**, 95 (1991).

[8] A. Georges and G. Kotliar, Phys. Rev. B **45**, 6479 (1992).

[9] M. Jarrell, Phys. Rev. Lett. **69**, 168 (1992).

[10] J. E. Hirsch and R. M. Fye, Phys. Rev. Lett. **56**, 2521 (1986).

[11] V. Zlatić and B. Horvatić, Solid State Commun. **75**, 263 (1990).

[12] E. Müller-Hartmann, Z. Phys. B **74**, 507 (1989); Z. Phys. B **76**, 211 (1989).

[13] M. Jarrell and Th. Pruschke, Z. Phys. B. **90**, 187(1993).

[14] W. H. Press, B. P. Flannery, S. A. Teukolsky, and W. T. Vetterling, *Numerical Recipes* (Cambridge University Press, Cambridge, 1986).

[15] Obeying causality is crucial to guarantee that the procedure described here is properly Herglotz.

[16] J. K. Freericks, M. Jarrell, and D. J. Scalapino, Phys. Rev. B **48**, 6302 (1993); *to appear in* Europhys. Lett. (1994)

[17] We would like to thank H.-B. Schüttler for suggesting we examine an effective phonon potential in this manner. See also J. Mustre de Leon, *et. al.* Phys. Rev. Lett. **68**, 3236 (1992); J. Zhong and H.-B. Schüttler, Phys. Rev. Lett. **69**, 1600 (1992).

[18] These results are qualitatively similar to those found in C. C. Yu and P. W. Anderson, Phys. Rev. B **29**, 6165 (1984).

[19] H. F. Trotter, Proc. Am. Math. Soc. **10** 545 (1959); M. Suzuki, Prog. Theor. Phys. **56**, 1454 (1976)

[20] J. E. Hirsch, Phys. Rev. B, **28**, 4059 (1983); **31**, 4403 (1985).